On the Prospects of BaF_2 as a Fast Scintillator for Time-of-Flight Positron Emission Tomography Systems

Katrin Herweg, *Graduate Student Member, IEEE*, Vanessa Nadig, *Graduate Student Member, IEEE*, Volkmar Schulz, and Stefan Gundacker, *Member, IEEE*

***Abstract*—Future time-of-flight positron emission tomography (TOF-PET) will be in need of ultrafast scintillation materials, with potential seen in cross-luminescence (CL). BaF_2, for example, shows a sub-100-ps decay time with 300 photons produced per MeV. However, it poses challenges, such as medium radiation length, low photofraction, moderate light yield, and vacuum ultraviolet (VUV) emission around 200 nm. Recent developments in UV-sensitive solid-state photodetectors (SiPMs) have the potential to establish CL for ultrafast TOF in PET. In this work, we aim to study BaF_2, read out by these new VUV SiPMs, as a viable alternative to cerium-doped lutetium–yttrium oxyorthosilicate (LYSO:Ce). In order to investigate the prospects of BaF_2 in TOF-PET, we compare the CTR of 2 × 2 × 20 mm^3 undoped and yttrium-doped BaF_2 crystals, readout by Hamamatsu S13370-3050CN SiPMs with a maximum photon detection efficiency (PDE) of 14% at 200 nm and air coupling, to LYSO:Ce:Ca crystals of the same size. With high-frequency readout electronics, we reached 233 ps with undoped BaF_2 and 213 ps with BaF_2:Y, while the performance of LYSO:Ce:Ca was 125 ps (measured with HPK S14160-3050HS, PDE ∼60% and glue coupling). Conducting measurements at different depth of interaction positions shows a pronounced impact on the CTR. Furthermore, we investigated the performance for systems of BaF_2 with TOFPET2c ASIC measurements and Geant4 simulations for effective sensitivity comparisons to LYSO:Ce:Ca.**

***Index Terms*—ASIC, BaF_2, cross-luminescence (CL), high-frequency (HF) readout, scintillator, TOF, TOFPET2.**

I. Introduction

TIME-OF-FLIGHT positron emission tomography (TOF-PET) is currently one of the research topics in medical imaging receiving considerable attention. Using a precise measurement of the arrival times of the gamma photons emitted in PET allows to increase the signal-to-noise ratio (SNR) of a PET system, thereby enabling a reduction of measurement time and tracer dosage beneficial to the patient. To achieve the most precise timing, ultrafast scintillator materials other than the state-of-the-art cerium-doped lutetium–yttrium oxyorthosilicate (LYSO:Ce) have been investigated, as its timing performance is limited due to the intrinsic timing limit of the cerium centers in LYSO:Ce, which lies at a decay time of 16 ns. This decay time imposes a limit on the achievable time resolution in PET, setting it at roughly 100-ps full width at half maximum (FWHM). In order to overcome this timing limit, other scintillation mechanisms have to be investigated [1], [2]. Studies in [3] have shown the potential of Cherenkov emission and BaF_2 for ultrafast high-rate time-of-flight applications and as a promising pathway to sub-100-ps PET.

Due to the higher amount of photons with sub-100 -ps decay time produced by cross-luminescence (CL) compared to, e.g., Cherenkov radiation (∼ 300 photons per MeV for CL in barium fluoride (BaF_2) and ∼ 33 photons per MeV for Cherenkov in bismuth germanate (BGO) [3]), we decided to focus on the CL-emitting BaF_2. The CL process only occurs in materials where the energy difference between the valence and core band is smaller than the band gap (see Fig. 1). When both core and valence band are fully populated and the conduction band is empty, the excitation of an electron from the core band into the conduction band is followed by the hole being filled with an electron from the valence band [5]. This results in the emission of a UV photon, which is extremely fast as no meta stable states are involved in the relaxation. The hole

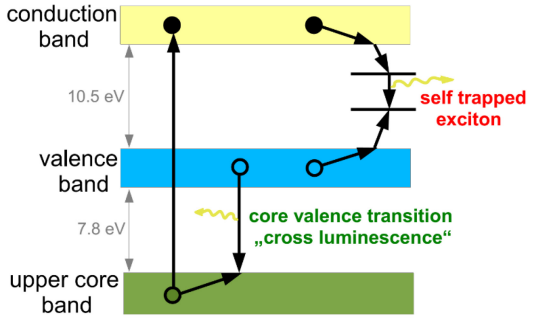

Fig. 1. Scheme of the scintillation process of BaF_2. Taken and adapted from [4], licensed under CC BY 3.0.

Manuscript received 26 November 2022; accepted 28 December 2022. Date of publication 18 January 2023; date of current version 3 March 2023. *(Volkmar Schulz and Stefan Gundacker share the last authorship.) (Corresponding authors: Katrin Herweg; Volkmar Schulz; Stefan Gundacker.)*

This work did not involve human subjects or animals in its research.

Katrin Herweg, Vanessa Nadig, and Stefan Gundacker are with the Department of Physics of Molecular Imaging Systems, Institute for Experimental Molecular Imaging, RWTH Aachen University, 52056 Aachen, Germany (e-mail: katrin.herweg@pmi.rwth-aachen.de; stefan.gundacker@pmi.rwth-aachen.de).

Volkmar Schulz is with the Department of Physics of Molecular Imaging Systems, Institute for Experimental Molecular Imaging, and the Physics Institute III B, RWTH Aachen University, 52056 Aachen, Germany, also with Hyperion Hybrid Imaging Systems GmbH, 52074 Aachen, Germany, and also with the Fraunhofer Institute for Digital Medicine MEVIS, 52074 Aachen, Germany (e-mail: volkmar.schulz@pmi.rwth-aachen.de).

Color versions of one or more figures in this article are available at https://doi.org/10.1109/TRPMS.2023.3237254.

Digital Object Identifier 10.1109/TRPMS.2023.3237254

in the valence band subsequently recombines with the excited electron via self-trapped exciton (STE) emission. While the CL provides a fast emission, at the same time, it poses one of the challenges of using BaF_2 as a scintillator in PET, as the emission in the vacuum ultraviolet (VUV) is hard to detect with mainstream photodetectors. Additional challenges are BaF_2's medium radiation length, low photofraction, and moderate light yield (see Table I), as well as its self-absorption of CL [6], [7] and mild hygroscopicity [7]. The medium radiation length and low photofraction of the crystal call for an increased crystal length in order to adequately absorb high energy particles, which makes the depth of interaction (DOI) an important and necessary information to reduce the parallax error in systems [8]. It could also help in improving the coincidence time resolution (CTR) via DOI-encoding [9]. Due to this need for increased crystal volume, BaF_2's potential for self-absorption, as noted, e.g., in [6], has to be considered. The disadvantages of BaF_2 are offset by its ultrafast emission and low production costs around \$15 per 1 cm^3 material [10], [11]. Since the main interest for the material lies in this ultrafast emission, it has been examined how to suppress the STE component of the scintillation emission through doping of the BaF_2 crystals [12], [13], [14], which is beneficial for high rate applications, e.g., TOF-CT [15], and, therefore, also in TOF-PET systems, especially, in view of real-time dose monitoring in hadron therapy. BaF_2 has been previously investigated in the 80s and 90s [6], [7], [16] and is currently regaining interest in the community due to new developments in photosensor and readout design, which make it possible to use BaF_2 crystals with SiPMs [10], [17].

In this work, we evaluate if BaF_2 in combination with these new SiPMs is a suitable material for TOF-PET system application by testing short and long BaF_2 crystal pixels on a power-efficient high-frequency (HF) setup [18], which allows to investigate the timing limits of the scintillator and photodetector. Additionally, we investigated the DOI dependence of the timing performance. We also examined the performance of BaF_2 with the TOFPET2c ASIC (PETsys Electronics S.A.), as this chip is suitable for system application, and conducted simulations to estimate the effective sensitivity of BaF_2 for different lengths and in comparison to LYSO:Ce:Ca and BGO. All measurements were similarly conducted with LYSO:Ce:Ca in order to compare to the current state of the art.

II. Materials and Methods

A. Scintillators and Photodetectors

In this study, we compared $2 \times 2 \times 3\,mm^3$ and $2 \times 2 \times 20\,mm^3$ BaF_2 and BaF_2:Y crystals (Epic Crystal, China) to similarly sized LYSO:Ce:Ca crystals ($2 \times 2 \times 3\,mm^3$ and $2 \times 2 \times 20\,mm^3$ by Taiwan Applied Crystal, China). The BaF_2 crystals were air-coupled to VUV SiPMs with an active area of $3 \times 3\,mm^2$ (S13370-3050CN, SPAD size 50 µm [24], by Hamamatsu Photonics K.K., Japan), while the LYSO crystals were readout by Broadcom SiPMs (AFBR-S4N33C013, SPAD size of 30 µm [25]) or S14160-3050HS Hamamatsu SiPMs (SPAD size 50 µm [26]) with the same active area. Additionally, the $2 \times 2 \times 3\,mm^3$ LYSO:Ce:Ca crystals were also tested air-coupled to the VUV SiPMs. Optical coupling for the LYSO crystals and Broadcom SiPMs was achieved with Meltmount ($n = 1.582$, Cargille, USA). For the S14160-3050HS Hamamatsu SiPMs air coupling as well as glue coupling with Meltmount was used. The length of 20 mm was chosen to correspond to clinical crystal specifications of LYSO-based systems [27]. All crystals were wrapped in several layers of Teflon tape.

TABLE I
Material Characteristics of BaF_2, LYSO, and BGO Values Are Taken From the Review of Particle Physics [19], Unless Otherwise Indicated

	BaF_2	**LSO:Ce**	**BGO**
density ($g\,cm^{-3}$)	4.88	7.4	7.13
Z_{eff}	53	66	75.2
radiation length (cm)	2	1.1	1.12
intrinsic light yield (ph/MeV)	1430[a] 9950[b]	27000	8200
decay time (ns)	0.6 – 0.8[a] 620[b]	40	300
photofraction at 511 keV	0.19 [20]	0.34 [20]	0.43 [20]
emission peak(s) (nm)	195[a] 220[a] 310[b]	420	505
refractive index at emission	1.56 [21] 1.55 [21] 1.50 [21]	1.82 [22]	2.14 [23]
melting point (°C)	1368	2150	1044
cost (\$/cm^3)	15 [11]	60 [11]	35 [11]

[a] cross luminescence
[b] self-trapped exciton emission

B. HF Setup

Determining the performance limits achievable for each detector assembly, we employed HF electronics similar to [28]. The HF circuit was connected to an oscilloscope (LeCroy Waverunner 9404M-MS, bandwidth 4 GHz, 20 GS/s) for digitization. In comparison to the original setup in [28], we employed less power-consuming BGA2851 amplifiers [18], but the same 3-GHz balun transformer (MABA-007159) in the timing channel as well as an AD8000 operational amplifier in the energy channel. The oscilloscope was configured to trigger on coincidences only. Both overvoltage and threshold scans are conducted as coincidence measurements [see Fig. 2(a)] and measurements against a reference detector [see Fig. 2(b)]. As the reference detector, a $2 \times 2 \times 3\,mm^3$ LYSO:Ce:Ca crystal coupled with Meltmount to a Broadcom SiPM was used.

For the 20 mm BaF_2, BaF_2:Y, and LYSO:Ce:Ca crystals, respectively, DOI measurements were conducted on the HF setup using electronic collimation. As seen in Figs. 2(c) and 3(a), this means positioning the crystals further apart than in the other setups and shifting the source as close as possible toward the 20-mm crystal. The distance between the reference detector and the source is about three times the distance between 20-mm crystal and source, which gives an illuminated region of roughly 0.7 mm. The $2 \times 2 \times 3\,mm^3$ LYSO:Ce:Ca crystals were used as a reference detector and both detectors

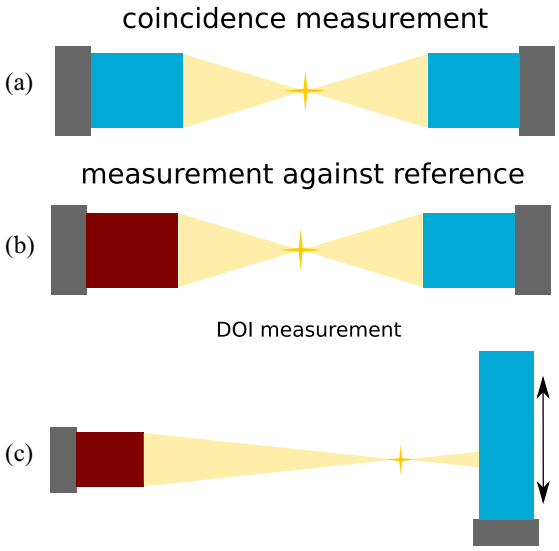

Fig. 2. Detector arrangements for the different measurements: (a) coincidence measurements, two detectors of the same build measured against each other with front irradiation; (b) measurement against reference, one detector as a reference (red) and a different detector under test (blue) measured with front irradiation; and (c) DOI measurement, a reference detector (red) measured against a detector with a long crystal in upright position (blue) for side irradiation and arranged for electronic collimation. For different DOI positions, it is shifted in front of the source as indicated by the arrow to the right.

were operated with optimal settings from the previous coincidence measurements. For the different DOI positions, the 20-mm crystal is shifted along its length in front of a stationary source and reference detector.

C. TOFPET2 ASIC Setup

To evaluate the performance of BaF_2 on system-scalable electronics, the 3-mm BaF_2 and LYSO:Ce:Ca detectors were also measured with the TOFPET2c ASIC by PETsys Electronics S.A. (standard settings for BaF_2: input stage impedance $R_{in} = 30\,\Omega$ [29], i.e., fe_ib1 = 57, vth_t1 = 1 with disc_lsb_t1 = 55, which sets the threshold step size to roughly 6.6 mV [29], vth_t2 = 20, vth_e = 15; for measurements with LYSO:Ce:Ca crystals, the input impedance is reduced to $R_{in} = 11\,\Omega$, i.e., fe_ib1 = 0). To allow a DC connection between SiPMs and the setup, the ASIC boards are connected with front-end and adapter boards, either provided by PETsys or custom-designed (see Fig. 3(b) as an example for the TOFPET2 ASIC setup).

The ASIC employs a three-threshold trigger logic for dark count rejection. Two of these thresholds (vth_t1 and vth_t2) are set for the signal in the timing branch, where the first threshold is set on a low threshold level to achieve the best possible timing and the second threshold is set on a higher scale and used as validation to reject dark counts. The third threshold (vth_e) is applied to the signal of the energy branch, which is mirrored from the input signal but amplified differently than the timing branch signal, as a further validation step. All thresholds are configured as unitless values and multiplied with a modifiable step width, e.g., disc_lsb_t1 for the step width of vth_t1.

Using this trigger logic and the ASIC's charge-integration mode (QDC mode), raw data were acquired and saved as a single information with timestamp, energy value, and channel-ID [29]. As coincidence measurements, we conducted both overvoltage and threshold scans.

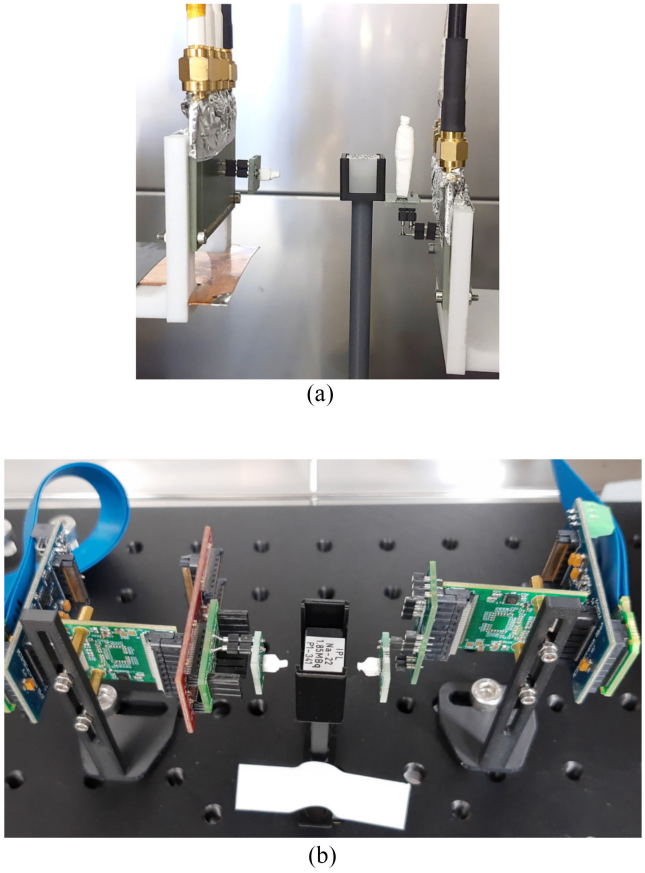

Fig. 3. Coincidence experiments. The HF readout can be seen in (a), where it is arranged for a DOI measurement with electronic collimation. (b) Shows TOFPET2 ASIC readout electronics.

All data were acquired by placing the setup in a climate chamber with an ambient temperature of 16 °C and using ^{22}Na sources with an active area of 0.25 or 0.5 mm and an activity of 0.5 MBq as well as 2.5 MBq.

D. Dark Count Scans

Scans to determine the dark count rate (DCR) of the SiPM samples were acquired for a VUV SiPM and an S14160-3050HS SiPM on both setups by counting the number of signals surpassing a single leading-edge trigger threshold. For this purpose, the three-threshold trigger logic of the TOFPET2 ASIC was reconfigured to a single-threshold trigger and the number of registered singles was saved. For the HF setup, a low leading-edge threshold of 20 mV was configured and a waveform for a time window of 2 ms was stored. The breakdown voltages of the measured SiPMs were determined with I-V-scans [30] to be 52.2 V for the VUV and 38.55 V for the S14160-3050HS SiPM. All dark count scans were conducted without crystals mounted to the SiPMs.

E. Geant4 Simulation Framework

We simulated single crystals of varying lengths and a 511-keV gamma impinging in the center of the surface with

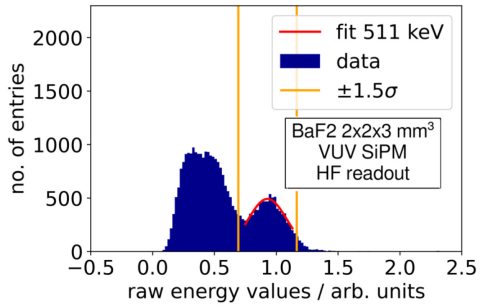

(a)

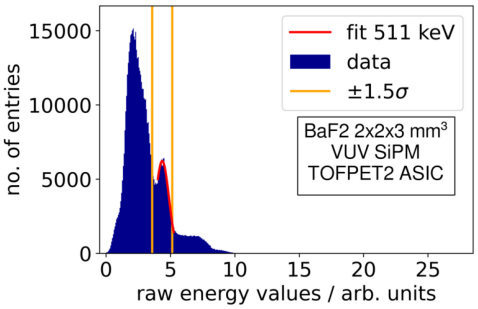

(b)

Fig. 4. Energy spectra of the $2 \times 2 \times 3\,\text{mm}^3$ BaF_2 crystals measured on the (a) HF setup and (b) ASIC setup at a bias voltage of 60 V, with a threshold of 100-mV for the HF measurement and 6.6 mV for the ASIC setup. The HF spectrum is a coincidence spectrum, while the ASIC shows a spectrum of only one detector.

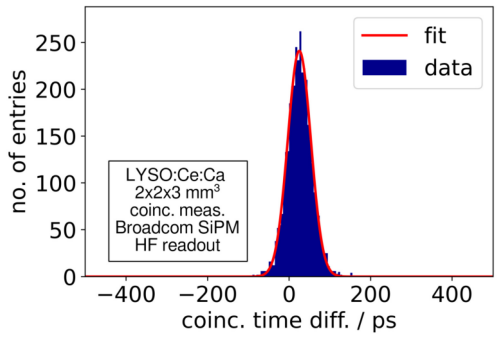

(a)

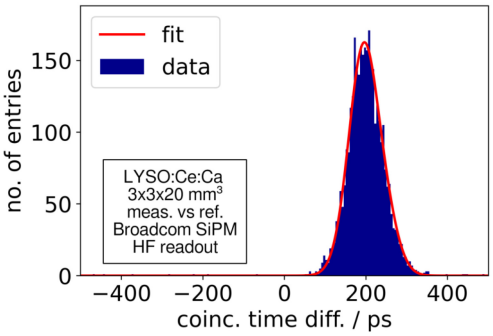

(b)

Fig. 5. Time difference spectra of the $2 \times 2 \times 3\,\text{mm}^3$ LYSO:Ce:Ca crystals measured on the HF setup, (a) in coincidence and (b) against a $3 \times 3 \times 20\,\text{mm}^3$ LYSO:Ce:Ca crystals at a bias voltage of 37 V, with a threshold of 100-mV.

nuclear physics interactions, using Geant4 (version 10.06.p03). With the same basic framework, we also simulated a detector ring with a geometry similar to the Siemens Biograph Vision (gantry size 78 cm, axial field of view (FOV) 26.4 cm, and crystal size $3.2 \times 3.2 \times 20$ mm [27]) and an isotropically emitting gamma point source. For both simulations, to estimate the effective sensitivity of BaF_2 in comparison to LSO, which is comparable to LYSO:Ce:Ca in this framework, we determined how many gammas deposited energy in the scintillator and normalized the number with the amount of gammas initially simulated.

F. Data Analysis

1) Coincidence Measurements: Since the TOFPET2 ASIC was used in singles acquisition mode, the singles have to be processed into coincidences. The singles acquired with the TOFPET2 ASIC were matched within a coincidence window of 3 ns. The photopeaks of the energy spectra (see Fig. 4) are fit with a Gaussian. Events are selected in a 1.5σ-environment around the 511-keV peak. For the $2 \times 2 \times 20\,\text{mm}^3$ BaF_2:Y crystal, a Gaussian fit was not possible due to insufficient peak separation [see Fig. 7(d)]. Therefore, a cutoff value is determined to select photopeak events and a photopeak position is roughly estimated. This is done by first fitting the Compton background and subtracting it, followed by selecting the point where the distribution falls off sharply again and determining the average between this point and the cutoff.

Afterward, the coincidence time difference spectrum is fit with a Gaussian and the CTR is determined as the FWHM of the fitted curve [see Fig. 5(a)]. For measurements against a reference detector, the time difference spectrum shows a slight asymmetry due to the different detector timing limits [see Fig. 5(b)]. In this case, a single Gaussian fit does not describe the distribution well. Therefore, a double Gaussian fit is applied and the starting parameters of one Gaussian are acquired from the left side and the other ones from the right side of the time difference spectrum. The FWHM of this fit is acquired numerically, while the CTR is again determined as the FWHM of the fitted curve. The mean time difference of the distribution is saved as the time skew for both the single and double Gaussian fit and considered for DOI measurements. Errors on the CTR are estimated by statistical means [31] and by repeated measurements. For measurements conducted with a reference detector, the CTR of the measurement (CTR_{meas}) is always corrected (CTR_{corr}) for the reference detector's CTR (CTR_{ref}) following

$$\text{CTR}_{\text{corr}} = \sqrt{2 \cdot \text{CTR}_{\text{meas}}^2 - \text{CTR}_{\text{ref}}^2}. \tag{1}$$

2) Dark Count Scans: For the dark count scans, the number of registered triggers was used to compute the DCR, which was then plotted against the threshold voltage. For the HF electronics, the registered triggers were determined by setting a voltage threshold on the stored waveform and counting the signal peaks surpassing the threshold.

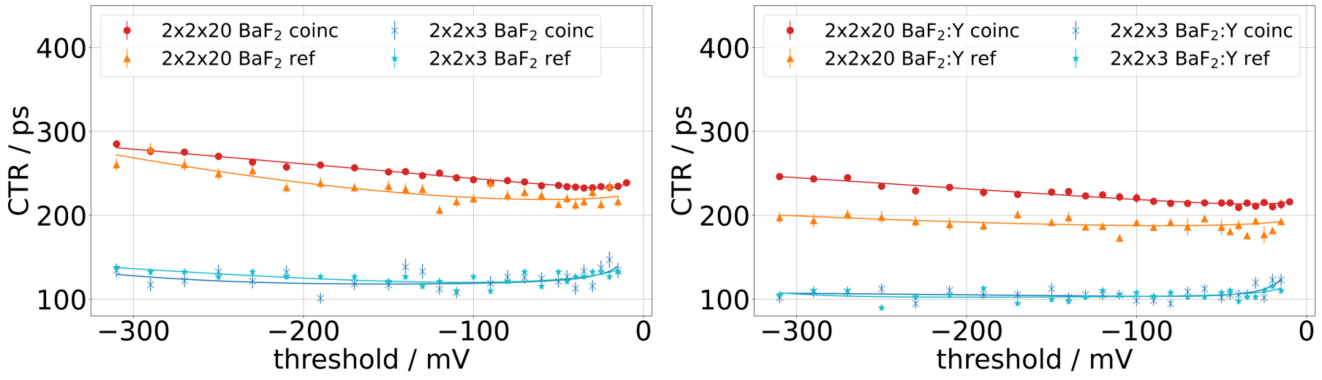

(a) (b)

Fig. 6. Threshold scans of the BaF_2 and BaF_2:Y detectors at 60-V bias voltage, displaying the CTR plotted against the threshold, comparing between measurements against a reference (ref), for which the CTR is reference-corrected, and measurements of two detectors under test in coincidence (coinc). In (a), the results for $2 \times 2 \times 3\,\mathrm{mm}^3$ and $2 \times 2 \times 20\,\mathrm{mm}^3$ undoped BaF_2 are presented. (b) Shows scans of $2 \times 2 \times 3\,\mathrm{mm}^3$ and $2 \times 2 \times 20\,\mathrm{mm}^3$ doped BaF_2:Y. No significant difference between the measurements for 3 mm can be found for either crystal. The difference between the 20 mm measurements is within $\pm 2\sigma$ environments at the minimum of the fitted curve.

TABLE II
OVERVIEW OF THE TIMING PERFORMANCE ACHIEVED WITH THE TWO RESPECTIVE SETUPS USED [28], [29] IN A COINCIDENCE MEASUREMENT AS DESCRIBED IN FIG. 2(a)

	HF readout	TOFPET2 ASIC
VUV SiPMs		
BaF_2 $2 \times 2 \times 3\,\mathrm{mm}^3$	118 ± 8	289 ± 21
BaF_2:Y $2 \times 2 \times 3\,\mathrm{mm}^3$	103 ± 6	–
LYSO:Ce:Ca $2 \times 2 \times 3\,\mathrm{mm}^3$	–	188 ± 8
BaF_2 $2 \times 2 \times 20\,\mathrm{mm}^3$	233 ± 3	–
BaF_2:Y $2 \times 2 \times 20\,\mathrm{mm}^3$	213 ± 4	–
Broadcom SiPMs		
LYSO:Ce:Ca $2 \times 2 \times 3\,\mathrm{mm}^3$	68 ± 1	125 ± 6
LYSO:Ce:Ca $3 \times 3 \times 20\,\mathrm{mm}^3$ glue-coupled	116 ± 2	–
S14160-3050HS SiPM		
LYSO:Ce:Ca $2 \times 2 \times 20\,\mathrm{mm}^3$ air-coupled (against reference)	181 ± 7	–
LYSO:Ce:Ca $2 \times 2 \times 20\,\mathrm{mm}^3$ glue-coupled	125 ± 8	–

Additionally, the derivative of the DCR is calculated and from the width of the resulting peaks as well as their distance, which describes the length of a DCR pedestal, an SNR estimate is made.

III. RESULTS

All results of CTR measurements conducted as coincidence measurements (arrangement (a) in Fig. 2) are summarized in Table II.

A. Timing Limits

1) Timing Performance: The best CTR for a $2 \times 2 \times 3\,\mathrm{mm}^3$ BaF_2 crystal, when measuring two BaF_2 crystals in coincidence, is (118 ± 8) ps [see Fig. 6(a)]. Measured against a reference detector of $2 \times 2 \times 3\,\mathrm{mm}^3$ LYSO:Ce:Ca coupled to a Broadcom SiPM (similar to [17]) the BaF_2 crystal reached (120 ± 4) ps [see Fig. 6(a)], with a bias voltage of 60 V and corrected for the reference time resolution of 68 ps according to (1). The $2 \times 2 \times 3\,\mathrm{mm}^3$ BaF_2:Y crystals reached a CTR of (103 ± 6) ps at 60-V bias voltage measured with two BaF_2:Y crystals in coincidence and (102 ± 4) ps for the same settings against the reference detector [see Fig. 6(b)]. The measurement of the LYSO:Ce:Ca reference detector has an optimal CTR of (68 ± 1) ps similar to measurements presented in [32].

Measuring two $2 \times 2 \times 20\,\mathrm{mm}^3$ BaF_2 crystals in coincidence shows a distinguishable Compton edge and photopeak, but the peak separation is significantly reduced for these longer crystals (see Fig. 7). The measurement in coincidence results in a CTR of (233 ± 3) ps and the measurement against reference yields (218 ± 6) ps [see Fig. 6(a)]. Measuring similarly with two $2 \times 2 \times 20\,\mathrm{mm}^3$ BaF_2:Y crystals, the energy spectrum shows no clearly resolvable peak anymore [see Fig. 7(d)], though a step in the histogram indicates the position of the photopeak and allows for an energy cut to be set. The CTR achieved with this filtering in a coincidence measurement lies at (213 ± 4) ps and at (187 ± 4) ps for a measurement against reference [see Fig. 6(b)]. In comparison, a measurement with a $2 \times 2 \times 20\,\mathrm{mm}^3$ LYSO:Ce:Ca crystal, glue-coupled to an S14160-3050HS SiPM and measured in coincidence, reaches (125 ± 8) ps and the reference-corrected CTR against a 3-mm LYSO:Ce:Ca crystal, glue-coupled to a Broadcom SiPM, as reference lies at (122 ± 5) ps. The air-coupled variant of this scintillator-detector combination reached a CTR of (181 ± 7) ps measured against reference.

2) DOI Measurements: The LYSO:Ce:Ca measurements ($2 \times 2 \times 20\,\mathrm{mm}^3$ crystals, wrapped in Teflon, readout by S14160-3050HS Hamamatsu SiPMs) show an improved CTR toward shallow (far away from the SiPM) and deep (close to the SiPM) DOI as well as values both above and below the CTR for front irradiation [see Fig. 8(a)]. For BaF_2, the CTR is best at the DOI position closest to the SiPM and deteriorates toward more shallow DOI. The deterioration stagnates after half of the crystal and the CTR stays constant. All results of the BaF_2 DOI measurements stay significantly

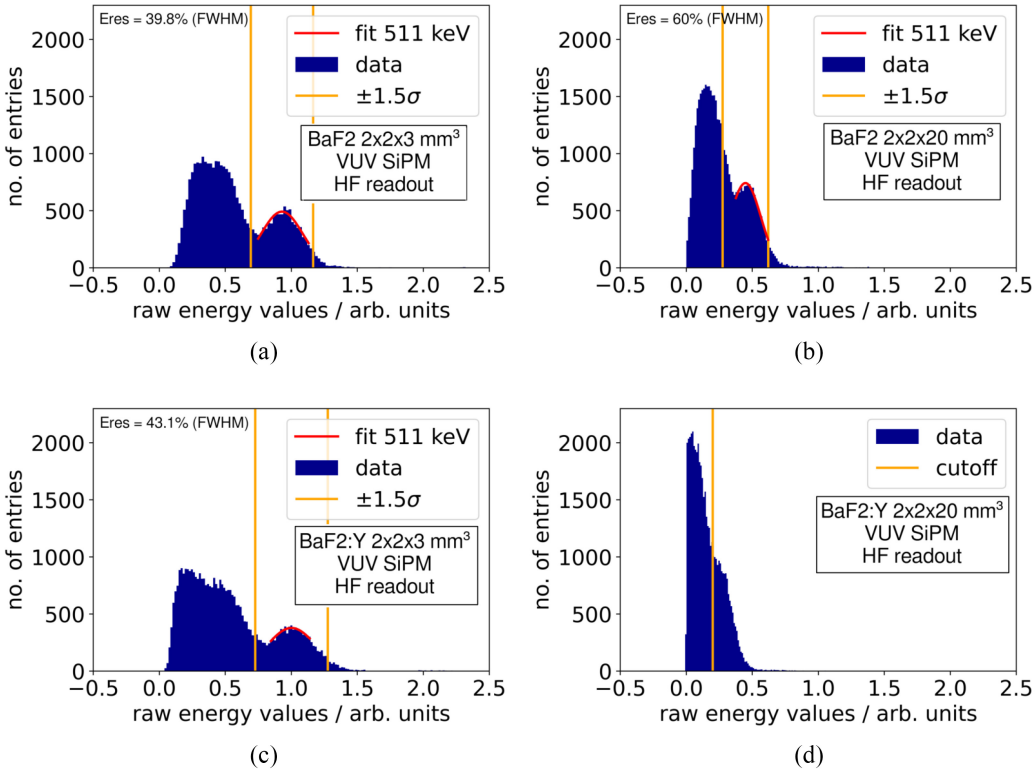

Fig. 7. Raw energy value spectra of (a) $2 \times 2 \times 3\,\mathrm{mm}^3$ and (b) $2 \times 2 \times 20\,\mathrm{mm}^3$ BaF_2 crystal and (c) $2 \times 2 \times 3\,\mathrm{mm}^3$ and (d) $2 \times 2 \times 20\,\mathrm{mm}^3$ BaF_2:Y crystal on HF setup at 60-V bias voltage, 100-mV threshold. The applied energy filter is shown in orange. For the $2 \times 2 \times 20\,\mathrm{mm}^3$ BaF_2:Y crystal, only a single cut was applied due to insufficient peak separation. The integration window for all crystals was set to ∼160 ns.

below the CTR values achieved with front-irradiation [see Fig. 9(a)]. BaF_2:Y, on the other hand, displays a maximum deterioration in the middle of the crystal while improving toward both ends. The front-irradiation CTR lies between the maximum and minimum CTR results for DOI measurements, similar to LYSO:Ce:Ca. The time skew of LYSO:Ce:Ca as well as doped and undoped BaF_2 shows a monotone decrease from shallow to deep DOI with a slight saturation at shallow DOI [see Figs. 8(b) and 9(b)]. Calculating the skew rate per millimeter for the region of the crystal not showing saturation (10–20 mm DOI), the LYSO detector achieves at maximum $(14.3 \pm 1.6)\,\mathrm{ps\,mm}^{-1}$ and at minimum $(6.3 \pm 1.8)\,\mathrm{ps\,mm}^{-1}$ for the air-coupled as well as $(14.1 \pm 0.2)\,\mathrm{ps\,mm}^{-1}$ and $(9.5 \pm 0.2)\,\mathrm{ps\,mm}^{-1}$ for the glue-coupled case while the undoped BaF_2 detector has a maximum rate of roughly $(11.2 \pm 0.2)\,\mathrm{ps\,mm}^{-1}$ and a minimum rate of $(6.7 \pm 3.5)\,\mathrm{ps\,mm}^{-1}$. The doped BaF_2:Y detector shows a maximum skew rate of around $(11.5 \pm 0.1)\,\mathrm{ps\,mm}^{-1}$ and a minimum skew rate of $(3.9 \pm 3.0)\,\mathrm{ps\,mm}^{-1}$. The photopeak position of the undoped BaF_2 is reduced by roughly 31 % over the whole DOI range [see Fig. 9(c)]. This effect is reduced to about 12 % for BaF_2:Y and is even slightly lower for LYSO:Ce:Ca [see Fig. 8(c)] with a difference of 8.9 % for the air-coupled and 8.4 % for the glue-coupled measurement.

B. Performance Tests for System Applicability

1) Timing Performance: Measuring the $2 \times 2 \times 3\,\mathrm{mm}^3$ LYSO:Ce:Ca crystals, readout by Broadcom SiPMs, on the ASIC setup results in a CTR of (125 ± 6) ps, which is in accord with the measurements in [32]. The results of BaF_2 show that a photopeak is visible in the energy spectra [see Fig. 4(b)] and has a sufficient separation from the Compton edge to do a peak fit and filter the data. The timing resolution of $2 \times 2 \times 3\,\mathrm{mm}^3$ undoped BaF_2 crystals achieved with the ASIC is severely degraded compared to the HF readout, reaching (289 ± 21) ps (see Fig. 10) with two identical detectors in coincidence at a bias voltage of 60 V and with a t1-threshold (see Section II-C) of 1.

To understand the deteriorated performance of the ASIC, we perform measurements of two LYSO:Ce:Ca crystals air-coupled to VUV SiPMs in coincidence (see Fig. 10). In these measurements, the best CTR achieved is (188 ± 8) ps. Furthermore, we evaluate dark count scans on both the HF and the TOFPET2 ASIC setup.

2) Dark Count Scans: The DCR scans are shown in Figs. 11 and 12. Their corresponding derivatives can be seen in Figs. 13 and 14. The DCR measured with the HF setup displays well distinguishable, flat pedestals for both the VUV SiPMs and the Hamamatsu S14160-3050HS, which represent the single-SPAD breakthrough of the detectors. The distance between these pedestals is larger for the VUV SiPMs [see Fig. 12(a)], while the number of pedestals visible is higher for the Hamamatsu S14160-3050HS [see Fig. 11(a)]. Indicating that the crosstalk between SPADs is significantly lower for the VUV SiPMs. In the derivative plots, we quantify the differences between the readouts by giving a rough estimate of the SNR as the ratio between pedestal length and step width

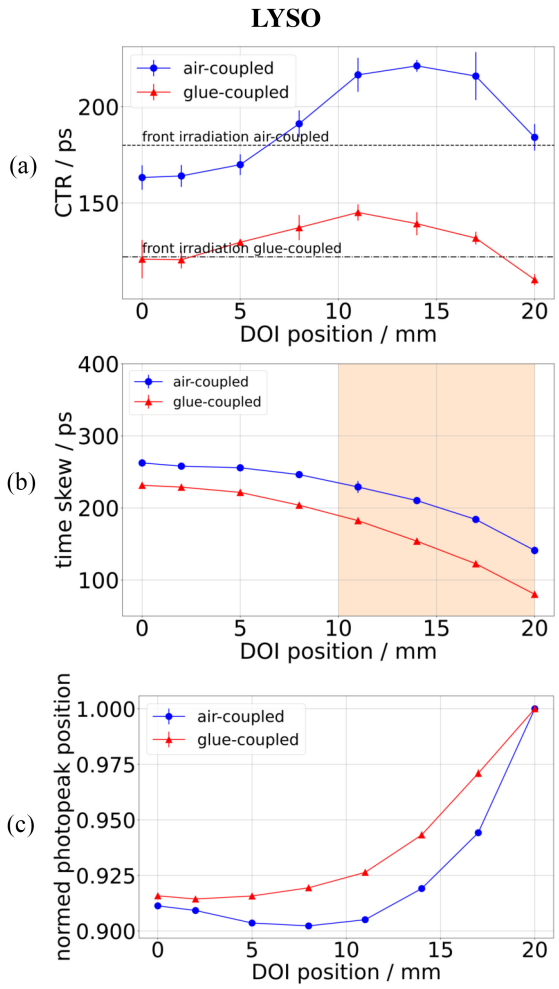

Fig. 8. Results of the DOI measurements for LYSO:Ce:Ca ($2 \times 2 \times 20\,mm^3$ crystals, Teflon-wrapped, readout by S14160-3050HS SiPMs), depicting the CTR in (a), the time skew in (b) and the photopeak position, normalized to its maximum, in (c), plotted against the DOI for a detector with air coupling and one with glue coupling. Here, DOI position zero is the position furthest from the SiPM. The CTR for front irradiation, measured against the reference, is shown as a dotted line. In (a), both measurements show a similar behavior, where the CTR deteriorates toward middle DOI and improves for shallow and deep DOI. The time skew in (b) decreases from shallow to deep DOI and saturates for more shallow DOI. In (c), the photopeak position is increased toward deeper DOI.

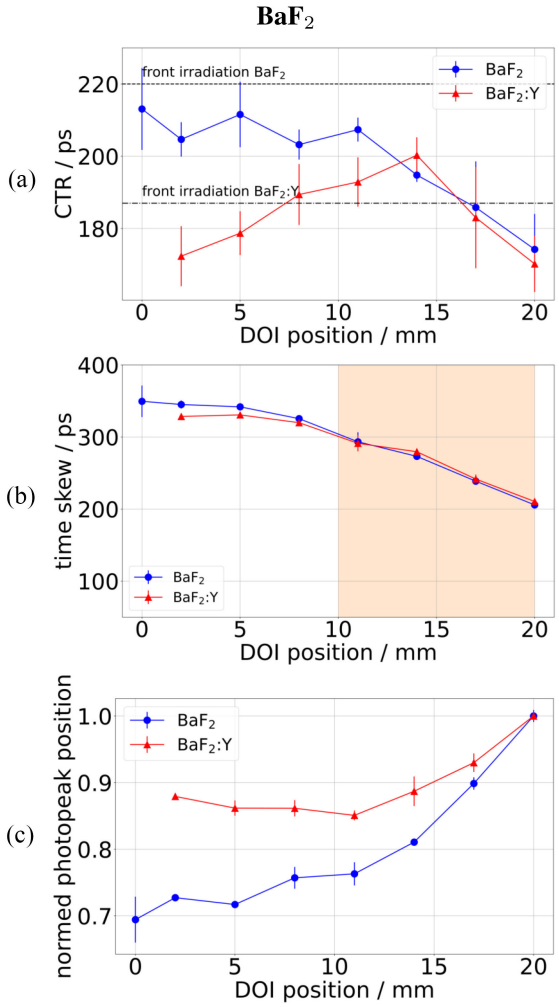

Fig. 9. Results of the DOI measurements for BaF_2 and BaF_2:Y ($2 \times 2 \times 20\,mm^3$ crystals, wrapped in Teflon, readout by VUV SiPMs), depicting the CTR in (a), the time skew in (b) and the photopeak position, normalized to its maximum, in (c), plotted against the DOI, respectively. Here, DOI position zero is the position furthest from the SiPM. The CTR for front irradiation, measured against the reference, is shown as a dotted line. For BaF_2, the CTR deteriorates for more shallow DOI additionally a lower photopeak is observed. The CTR for BaF_2:Y shows the highest degradation in the middle of the crystal and an improvement of CTR toward both shallow and deep DOI positions.

(FWHM of peaks in the derivative plot). For the HF electronics and the Hamamatsu S14160-3050HS an SNR of about 3.1 was achieved for an overvoltage of 3.45 V (SNR of ~5.7 for overvoltage 7.45 V). On the TOFPET2 ASIC, we reached an SNR of around 1.8 for an overvoltage of 3.45 V (SNR of ~3.1 for overvoltage 7.45 V). For the VUV SiPMs measured on the TOFPET2 ASIC, the single-SPAD pedestals can essentially not be resolved anymore. Only a slight bend in the curve is visible [see Fig. 12(b)]. In the derivative curve, it is not possible to estimate the FHWM of the peaks, which can be barely distinguished [see Fig. 14(b)].

3) Geant4 Simulation Framework and Effective Sensitivity: We determined the effective sensitivity by counting the gammas depositing energy in the scintillator and dividing this number by the total number of gammas created. The results can be seen in Fig. 15. It becomes evident that BaF_2 needs to be roughly twice as long as LSO in order to show the same gamma detection efficiency.

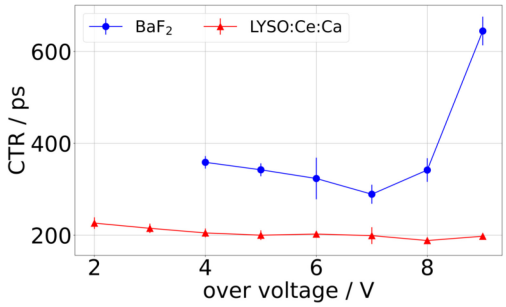

Fig. 10. Overvoltage and threshold scan of $2 \times 2 \times 3\,mm^3$ BaF_2 and LYSO:Ce:Ca crystals, both air-coupled to VUV SiPMs, measured with the TOFPET2 ASIC with an input impedance of 30 Ω (fe_ib1 = 57) for BaF_2 and 11 Ω (fe_ib1 = 0) for LYSO:Ce:Ca.

To go for a simulation closer to a real system, we went from the single crystal simulation to a whole detector ring. When moving the gamma source through the axial FOV of a detector ring, modeled after the Siemens Biograph Vision,

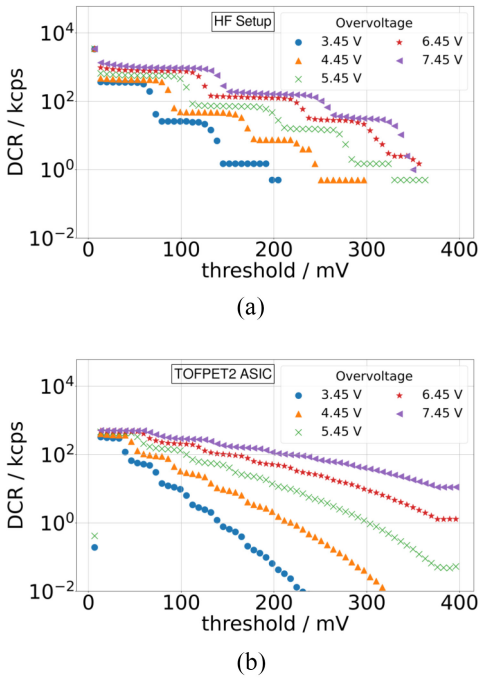

Fig. 11. DCR plots against the leading-edge threshold for a Hamamatsu S14160-3050HS SiPM on different setups: (a) on HF setup and (b) on TOFPET2 ASIC setup. The first threshold in (b) is triggering in the electronic noise and reaches the maximum output of the ASIC.

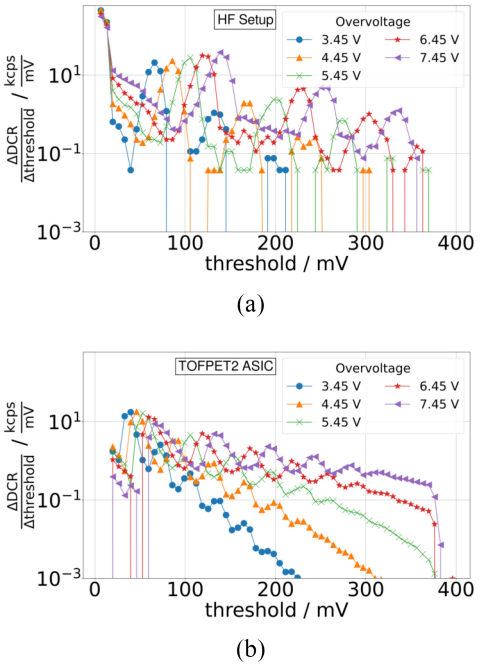

Fig. 13. Derivative of DCR plots against the leading edge threshold for a Hamamatsu S14160-3050HS SiPM on different setups: (a) on HF setup and (b) on TOFPET2 ASIC setup. Both graphs show distinct peaks in a Gaussian shape.

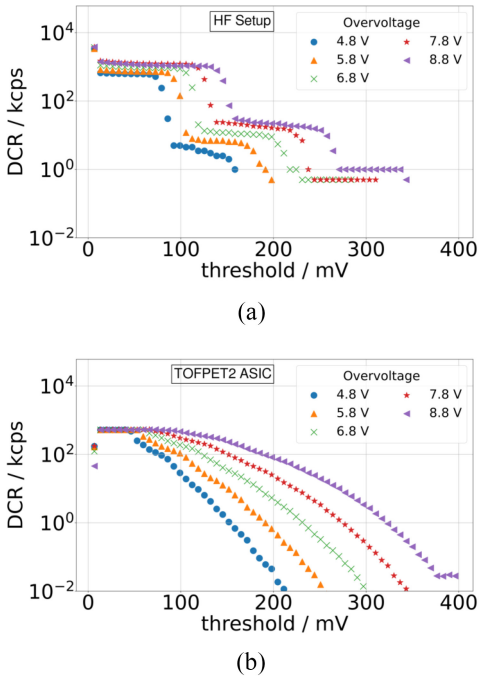

Fig. 12. DCR plots against the leading edge threshold for a VUV SiPM on different setups: (a) on HF setup and (b) on TOFPET2 ASIC setup. The first threshold in (b) is triggering in the electronic noise and reaches the maximum output of the ASIC.

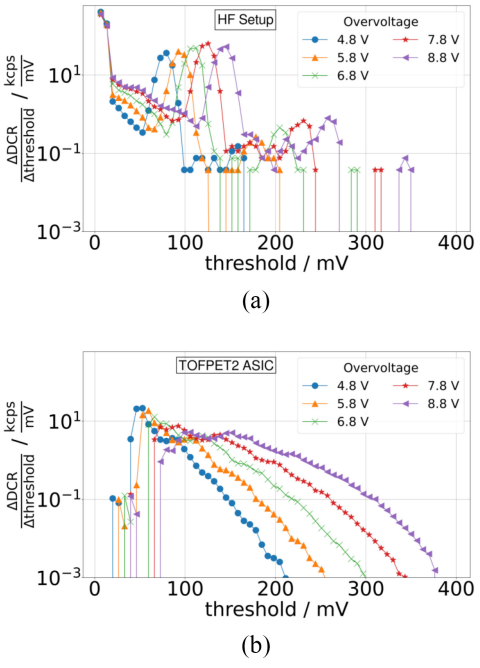

Fig. 14. Derivative of DCR plots against the leading edge threshold for a VUV SiPM on different setups: (a) on HF setup and (b) on TOFPET2 ASIC setup. While (a) shows distinct peaks in a Gaussian shape, in (b), no clear peaks can be distinguished.

the simulations show the expected behavior of decreasing sensitivity toward the edges of the FOV (see Fig. 16). An increased sensitivity for crystals with lower radiation length and higher photofraction of the same length or higher length crystals of the same radiation length and photofraction is observed. It is confirmed that the BaF_2 needs to be twice the length of LSO for the same overall sensitivity. Only considering photopeak events [see Fig. 16(b)], the difference in radiation length becomes more pronounced and the higher probability for Compton scatter in BaF_2 causes the amount of necessary material to rise to 50 mm. We have also included an example of 20-mm BGO in the detector ring simulation.

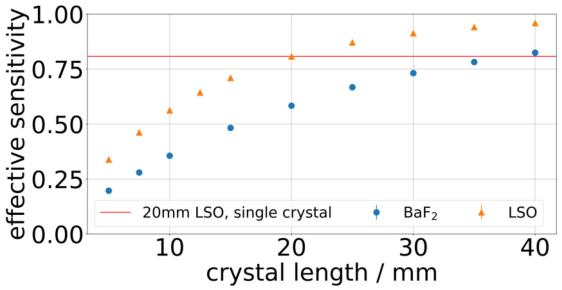

Fig. 15. Geant4 simulations of single crystals of LSO and BaF_2 to compare effective sensitivity of the materials for different lengths.

The BGO curve exceeds both the LSO and BaF_2 curves [see Fig. 16(a)].

IV. Discussion

Performance limits for the timing were determined for all BaF_2 detector configurations in coincidence measurements of two identical detectors and where possible compared to [17]. Additionally, a comparison to a system-applicable ASIC readout was conducted.

A. Timing Limits

1) Timing Performance: The comparison to the literature showed that the results of our undoped BaF_2 samples are degraded by roughly 20% compared to the literature, where (98 ± 5) ps [17] are stated, but the results of the BaF_2:Y samples are in accordance. Since yttrium doping is only meant to suppress the STE emission and not enhance the timing performance, which was also shown in [10], we conclude that the measured undoped BaF_2 crystals have a poorer intrinsic timing than the ones measured in [17]. We also showed that for $2 \times 2 \times 3\,\text{mm}^3$ crystals measuring against a reference detector does not affect the BaF_2 detector's timing performance compared to coincidence measurements.

When comparing the BaF_2 and the LYSO measurements, the measurements of doped and undoped BaF_2 crystals are outperformed by the LYSO:Ce:Ca detectors. But it has to be noted that the LYSO measurements were taken with an optimized optical coupling and a photodetector, whose photon detection efficiency (PDE) at LYSO emission wavelength (∼54 % at 420 nm [25], see Fig. 17) is about three times the one of the Hamamatsu VUV SiPM at the fast scintillation wavelength of BaF_2 (∼15 % at 178 nm [33], see Fig. 17). Additionally, BaF_2 was measured air-coupled. Therefore, finding an optical coupling material with a suitable refractive index and high transmissivity as well as improving the PDE of the VUV SiPM will certainly boost the performance and system applicability of BaF_2. Using the following equation from [3]:

$$\text{CTR}_{\text{analytic}} = \frac{3.33}{\sqrt{\text{PDE} \cdot \text{LTE} \cdot \text{IPTD}}} \tag{2}$$

where LTE denotes the light transfer efficiency and IPTD the crystal's initial photon-time density, it can be calculated that improving the PDE for the VUV SiPMs alone from 15% to 54% should improve the CTR by a factor of ∼1.9. Another

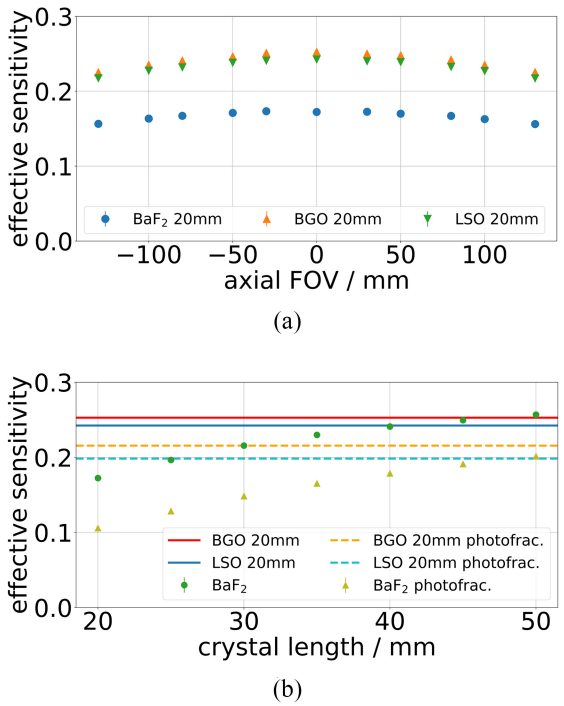

Fig. 16. Simulations of a gantry are shown. The source was moved through the axial FOV and the effective sensitivity is displayed for a 20-mm BaF_2 crystal in comparison with a 20-mm LSO and BGO crystal in (a). (b) Only the FOV position 0 mm for several different lengths of BaF_2 with again the values of 20-mm LSO and BGO as comparison. While one dataset shows all events detected, the other only considers events for which 511 keV are deposited in the gantry (photo frac.).

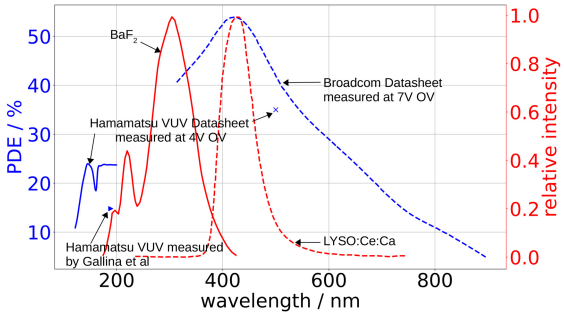

Fig. 17. Overlay of PDE and scintillation emission spectra for BaF_2 (red, solid line) and VUV SiPMs (blue, solid line) as well as LYSO:Ce:Ca (red, dashed line) and the used Broadcom SiPMs (blue, dashed line). Both PDE spectra have been taken from their respective datasheets [24], [25]. In measurements by Gallina et al. [33], it was shown that the PDE of the VUV SiPMs as stated in the datasheet is overestimated.

improvement could be made by changing the wrapping material, as Teflon seems to become more transparent for deep UV light [3], [34]. Considering all this, the results of the 3-mm BaF_2 and BaF_2:Y crystals show promise for sub-100-ps timing performance, also for longer crystals as suggested in [10].

For the 20-mm crystals, the measurement against reference shows a slightly better CTR performance compared to the coincidence measurements, though the difference is not overly significant, being within two sigma environments of each others error. Nevertheless, such a result could be expected, as it can be explained by a DOI-induced time bias, which is reduced for measurements against a short reference detector [9]. The results of the long crystals at ∼230 ps (BaF_2) and ∼210 ps

TABLE III
MEASUREMENT AGAINST REFERENCE OF 20-MM BaF_2 CRYSTALS WITH DIFFERENT WRAPPINGS, AIR-COUPLED TO VUV SIPMS. THE REFERENCE DETECTOR IS A $2 \times 2 \times 3\,mm^3$ LYSO:CE:CA CRYSTAL GLUED TO BROADCOM SIPMS WITH CARGILLE MELTMOUNT. ESR FOIL AND $BaSO_4$ WERE BY SICHUAN TIANLE PHOTONICS COMPANY LTD. (CHINA). ALL CTRS REPORTED ARE CORRECTED FOR THE REFERENCE

no wrapping	Teflon™	ESR	$BaSO_4$
223 ± 5 ps	221 ± 3 ps	226 ± 13 ps	220 ± 7 ps

(BaF_2:Y), compared to those of the short crystals at ∼120ps (BaF_2) and ∼100ps (BaF_2:Y), confirm that the performance of doped and undoped BaF_2 deteriorates with growing crystal length [35]. This suggests a degraded light transport within the BaF_2 crystals. The wrapping with Teflon could have an additional effect for the 20-mm long crystals, due to its transmissivity for VUV light, as mentioned before. By also testing ESR wrapping and $BaSO_4$ coating as well as no wrapping, we confirmed that none of the three wrapping methods improved the timing performance compared to the naked crystal (see Table III). Therefore, we assume that the wrapping methods tested are not reflective for the fast emission of BaF_2. A suitable coupling agent also has a high influence on the timing performance, as seen when comparing the air-coupled and glue-coupled LYSO:Ce:Ca measurements [see Table II and Fig. 8(a)]. We would also like to stress that the timing difference between the air-coupled LYSO:Ce:Ca crystals with a photodetector with higher PDE and the BaF_2:Y crystals is only 30 ps, showing that we have a high potential for improvement with a good coupling medium and higher PDE for the VUV SiPMs.

2) DOI Measurements: The behavior for a DOI measurement, as expected from light propagation theory, is described in [9] and [35]. A deteriorated CTR can be expected somewhere in the middle of the crystal, while it improves toward both ends of the crystal. This is due to the different paths that optical photons travel, when emitted in direction of the photodetector or in the opposite direction. If the DOI is very shallow or very deep, the timely difference between the two photon waves is almost zero or the largest and has, therefore, no influence or can be distinguished by fast electronics. In the middle of the crystal, however, this distinction is not possible and due to a finite single-photon time resolution (SPTR), the two photon waves are overlapping and lead to worse timing. The behavior described before can be seen in both the LYSO:Ce:Ca and the BaF_2:Y measurements.

For the undoped BaF_2 measurements, we observe a flattening of the CTR curve toward shallow DOI, which suggests that there is a significant amount of absorption in this crystal. This is further supported by the comparison of the photopeak positions in Fig. 6.

Comparing the results of the front-irradiation measurement to those at different DOI positions, for LYSO:Ce:Ca and BaF_2:Y, the front irradiation has a CTR value roughly fitting to the mean of the different DOI measurements. For undoped BaF_2 on the other hand, the front-irradiation CTR stays above all DOI measurements. Since the front-irradiation can be understood as an average of all the different DOI positions with a weighting of the position according to the attenuation probability, it seems plausible to have the measured CTR of front-irradiation as the mean of the different DOI positions shifted slightly toward the values of more shallow DOI (due to the exponential gamma absorption). The behavior of undoped BaF_2 can be explained by considering the distribution of time skews in combination with the flattening of the CTR curve for shallow DOI. More events are stopped in the first half of the crystal, where their CTR lies around 210 ps [see Fig. 9(a)], at the same time, the time skew of their time difference distributions already differ by ∼50 ps. Combining these events in a front irradiation measurement will lead to a broader time difference spectrum than for a single DOI position. Additionally, the significant light loss seen in Fig. 9(c) also contributes to this by causing time walk effects.

Optical theory suggests that a photon traveling 1 mm in a material should do so with the material-specific velocity of light. For LYSO (refractive index $n = 1.82$), this means the time taken per millimeter material should be $6.1\,ps\,mm^{-1}$ and for BaF_2 (refractive index $n = 1.53$), this equates to $5.1\,ps\,mm^{-1}$. The time skew curves show that we have a significant flattening of the curve for shallow DOI in all materials. Therefore, we only considered the skew rate for DOI between 10 and 20 mm. The minimal skew rates are close to the theory within their errors for all measurements except for the glue-coupled LYSO measurement. We expect the glue-coupled detector to have a longer photon transit time, as the light can have a different exit angle due to the glue's refractive index, which allows the SiPM to detect photons with longer travel path in the crystal.

The absorption in the undoped BaF_2 is additionally visible in the significant shift of the photopeak position for this crystal. The photopeak shift is reduced by roughly a factor of two for the doped BaF_2:Y crystal, which also displays a better timing performance. Further supporting the assumption that the absorption in the doped material is significantly reduced compared to the undoped BaF_2 crystal.

With the dependency of the CTR on the DOI, a correction of the CTR with the DOI position could provide improved timing, which would be, especially, beneficial for long crystals.

B. Performance Tests for System Applicability

1) Timing Performance: The performance of the BaF_2 detector in combination with the ASIC is severely degraded compared to the HF setup. Some degradation could be expected, as it is also observed for LYSO detectors (see Table II), but while the LYSO measurements on different setups deteriorate from 68 to 125 ps, the CTR for BaF_2 shows a larger degradation from 118 to 289 ps. One reason for this degradation can be seen in the results from the DCR scans. When comparing the results for the HF setup with the TOFPET2 ASIC setup considering Hamamatsu S14160-3050HS SiPMs, it can be seen that the TOFPET2 ASIC provides an almost two times lower SNR based on the ratio between the length of the pedestals and the FWHM of the peaks in the derivative of the staircase plots (see Fig. 14).

For the VUV SiPMs on the TOFPET2 ASIC setup it is not possible to calculate the SNR since the pedestals are not clearly distinguishable anymore, suggesting a severely degraded SNR.

2) Geant4 Simulation Framework and Effective Sensitivity: It was shown that in order to achieve an effective sensitivity similar to 20-mm LSO crystals in single crystals as well as in a detector ring a BaF_2 crystal will have to be twice as long as the LSO crystals. In the detector ring simulation, it was also demonstrated, that, if a length of 50-mm BaF_2 is chosen, even the sensitivity of BGO can be reached. If the fraction of photopeak events is also taken into consideration, however, the factor of two between LSO and BaF_2 increases to 2.5, due to BaF_2's high probability for Compton scatter. The performance of BGO surpasses both LSO and the simulated BaF_2 lengths significantly, but BGO only produces a marginal number of ultrafast photons, posing a huge disadvantage despite its low radiation length and high photofraction.

Taking into account the length a BaF_2 crystal would have to have for a TOF-PET system with effective sensitivity similar to LSO and how much the CTR of the 20-mm BaF_2 and BaF_2:Y crystals is degraded compared to the 3-mm crystals, it becomes clear, that without DOI encoding the timing performance cannot be up to par with available LYSO systems. Additionally, such long crystals would also introduce a large parallax error in a PET ring, further motivating the need for DOI encoding in a BaF_2 detector for a TOF-PET system or the use of alternative geometries, e.g., double-sided readout [36]. Approaches like the double-sided readout and detector arrangements as described in [36] could also solve issues surrounding the self-absorption probability for very long crystals.

From a financial point of view, 2.5 times the amount of BaF_2 would still be 1.6 times cheaper than LYSO, which has a roughly four times higher cost in production compared to BaF_2 [10], [11] due to lower raw material cost and lower melting point (see Table I). To build a scanner, it would have to be taken into account that for the same transaxial FOV the outer diameter of the scanner would have to be increased by 6 cm.

V. Conclusion

We evaluated the potential suitability of BaF_2 for system application in TOF-PET. It was found that single-channel BaF_2/BaF_2:Y crystals with lengths of 20 mm reach a CTR of (233 ± 3) ps/(213 ± 4) ps employing currently commercially available VUV SiPMs from Hamamatsu, showing a PDE of only 15% at ∼200 nm as compared to 54 % for LYSO compatible NUV SiPMs at 420 nm. When comparing the CTR deterioration from 3 to 20 mm crystals and considering the DOI measurements, it seems that the measured BaF_2 samples probably exhibit a higher absorption for optical photons than LYSO:Ce:Ca. Simulating the effective sensitivity pointed out that, for a sensitivity similar to LYSO, BaF_2 crystals would have to be twice or more the length of LYSO. Therefore, a tradeoff between low cost and high sensitivity is necessary, which at this point is still in favor of BaF_2 with a cost reduction of a factor of 1.6 for the case of a 50-mm BaF_2 crystal compared to a 20-mm LYSO crystal. This also highly motivates a DOI encoding for a BaF_2 detector. Trying to read out the BaF_2 crystals with a system-applicable TOFPET2 ASIC showed performance loss, caused most probably by the lower SNR of the ASIC. Overall, with the results achieved so far, there are various open points of research, like suitable readout electronics, good optical coupling and wrapping, and an improved PDE of VUV SiPMs. If these points can be addressed, we see potential for the use of BaF_2 crystals in TOF-PET.

Acknowledgment

The authors declare the following financial interests/personal relationships which may be considered as potential competing interests with the work reported in this article: Volkmar Schulz is the Co-Founder and an Employee of the spin-off company Hyperion Hybrid Imaging Systems GmbH, Aachen, Germany.

The authors would like to thank Mitch Chou from National Sun Yat-sen University and Jack Lin and Edmund Chin from Taiwan Applied Crystals for providing the LYSO:Ce:Ca samples.

References

[1] P. Lecoq, "Pushing the limits in time-of-flight PET imaging," *IEEE Trans. Radiat. Plasma Med. Sci.*, vol. 1, no. 6, pp. 473–485, Nov. 2017.

[2] P. Lecoq et al., "Roadmap toward the 10 ps time-of-flight PET challenge," *Phys. Med. Biol.*, vol. 65, no. 21, 2020, Art. no. 21RM01.

[3] S. Gundacker et al., "Experimental time resolution limits of modern SiPMs and TOF-PET detectors exploring different scintillators and Cherenkov emission," *Phys. Med. Biol.*, vol. 65, no. 2, 2020, Art. no. 25001.

[4] S. Diehl, R. W. Novotny, B. Wohlfahrt, and R. Beck, "Readout concepts for the suppression of the slow component of BaF_2 for the upgrade of the TAPS spectrometer at ELSA," in *Proc. J. Phys. Conf.*, vol. 587, 2015, Art. no. 12044.

[5] C. W. E. van Eijk, "Cross-luminescence," *J. Lumin.*, vols. 60–61, pp. 936–941, Apr. 1994.

[6] W.-H. Wong, N. A. Mullani, G. Wardworth, R. K. Hartz, and D. Bristow, "Characteristics of small barium fluoride (BaF_2) scintillator for high intrinsic resolution time-of-flight positron emission tomography," *IEEE Trans. Nucl. Sci.*, vol. 31, no. 1, pp. 381–386, Feb. 1984.

[7] Z. Y. Wei, R. Y. Zhu, H. Newman, and Z. W. Yin, "Light yield and surface treatment of barium fluoride crystals," *Nucl. Instrum. Methods Phys. Res. B*, vol. 61, no. 1, pp. 61–66, 1991.

[8] D. L. Bailey, D. W. Townsend, P. E. Valk, and M. N. Maisey, *Positron Emission Tomography*. London, U.K.: Springer, 2005.

[9] F. Loignon-Houle et al., "DOI estimation through signal arrival time distribution: A theoretical description including proof of concept measurements," *Phys. Med. Biol.*, vol. 66, no. 9, 2021, Art. no. 95015.

[10] S. Gundacker et al., "Vacuum ultraviolet silicon photomultipliers applied to BaF_2cross-luminescence detection for high-rate ultrafast timing applications," *Phys. Med. Biol.*, vol. 66, no. 11, 2021, Art. no. 114002.

[11] S. I. Eidelman and B. A. Shwartz, *Interactions of Particles and Radiation with Matter*. Berlin, Germany: Springer, 2012, pp. 3–23. [Online]. Available: https://doi.org/10.1007/978-3-642-13271-1_1

[12] C. L. Woody, P. W. Levy, and J. A. Kierstead, "Slow component suppression and radiation damage in doped BaF_2 crystals," *IEEE Trans. Nucl. Sci.*, vol. 36, no. 1, pp. 536–542, Feb. 1989.

[13] P. A. Rodnyi, M. A. Terekhin, and E. N. Mel'chakov, "Radiative core-valence transitions in barium-based fluorides," *J. Lumin.*, vol. 47, no. 6, pp. 281–284, 1991.

[14] C. Hu, C. Xu, L. Zhang, Q. Zhang, and R. Y. Zhu, "Development of yttrium-doped BaF_2 crystals for future HEP experiments," *IEEE Trans. Nucl. Sci.*, vol. 66, no. 7, pp. 1854–1860, Jul. 2019.

[15] J. Rossignol et al., "Time-of-flight computed tomography—Proof of principle," *Phys. Med. Biol.*, vol. 65, no. 8, 2020, Art. no. 85013.

[16] M. Laval et al., "Barium fluoride—Inorganic scintillator for subnanosecond timing," *Nucl. Instrum. Methods Phys. Res.*, vol. 206, nos. 1–2, pp. 169–176, 1983.

[17] R. H. Pots, E. Auffray, and S. Gundacker, "Exploiting cross-luminescence in BaF_2 for ultrafast timing applications using deep-ultraviolet sensitive HPK silicon photomultipliers," *Front. Phys.*, vol. 8, pp. 1–11, Oct. 2020.

[18] M. Krake, V. Nadig, V. Schulz, and S. Gundacker, "Power-efficient high-frequency readout concepts of SiPMs for TOF-PET and HEP," *Nucl. Instrum. Methods Phys. Res. A, Accelerators Spectrometers Detect. Assoc. Equip.*, vol. 1039, Sep. 2022, Art. no. 167032. [Online]. Available: https://www.sciencedirect.com/science/article/pii/S0168900222004570

[19] P. Lecoq, M. Korzhik, and A. Gektin, *Inorganic Scintillators for Detector Systems Physical Principles and Crystal Engineering Second Edition*. Cham, Switzerland: Springer, 2017. [Online]. Available: http://www.springer.com/series/5267

[20] S. Derenzo. "The quest for new radiation detector materials." 2008. Accessed: Nov. 8, 2022. [Online]. Available: https://www-group.slac.stanford.edu/ais/publicDocs/presentation88.pdf

[21] H. H. Li, "Refractive index of alkaline earth halides and its wavelength and temperature derivatives," *J. Phys. Chem. Ref. Data*, vol. 9, no. 1, pp. 161–290, 1980.

[22] R. Mao, L. Zhang, and R.-Y. Zhu, "Optical and scintillation properties of inorganic scintillators in high energy physics," *IEEE Trans. Nucl. Sci.*, vol. 55, no. 4, pp. 2425–2431, Aug. 2008.

[23] P. A. Williams, A. H. Rose, K. S. Lee, D. C. Conrad, G. W. Day, and P. D. Hale, "Optical, thermo-optic, electro-optic, and photoelastic properties of bismuth germanate (Bi4Ge3O12)," *Appl. Opt.*, vol. 35, no. 19, pp. 3562–3569, Jul. 1996. [Online]. Available: https://opg.optica.org/ao/abstract.cfm?URI=ao-35-19-3562

[24] "VUV-MPPC 4th generation (VUV4)," Data Sheet, Hamamatsu Photon. K.K., Hamamatsu, Japan, 2017.

[25] "NUV-HD single silicon photo multiplier," Data Sheet AFBR-S4N33C013, Broadcom, San Jose, CA, USA, 2022.

[26] *Hamamatsu MPPC*, Hamamatsu Photon. K.K., Hamamatsu, Japan, 2020.

[27] *Biograph Vision Technical Flyer*, Siemens Healthcare GmbH, Erlangen, Germany, 2018. [Online]. Available: https://www.healthcare.siemens.de/molecular-imaging/pet-ct/biograph-vision

[28] S. Gundacker, R. M. Turtos, E. Auffray, M. Paganoni, and P. Lecoq, "High-frequency SiPM readout advances measured coincidence time resolution limits in TOF-PET," *Phys. Med. Biol.*, vol. 64, no. 5, 2019, Art. no. 55012.

[29] *TOFPET 2C/D SiPM Readout ASIC*, PETsys Electronics S.A., Porto Salvo, Portugal, 2020.

[30] F. Acerbi and S. Gundacker, "Understanding and simulating SiPMs," *Nucl. Instrum. Methods Phys. Res. A, Accelerators Spectrometers Detect. Assoc. Equip.*, vol. 926, pp. 16–35, May 2019. [Online]. Available: https://doi.org/10.1016/j.nima.2018.11.118

[31] S. Ahn and J. A. Fessler, "Standard errors of mean, variance, and standard deviation estimators," Dept. Electr. Eng. Comput. Sci., Univ. Michigan, Ann Arbor, MI, USA, Rep. 413, 2003.

[32] V. Nadig et al., "A comprehensive study on the timing limits of the TOFPET2 ASIC and on approaches for improvements," *IEEE Trans. Radiat. Plasma Med. Sci.*, vol. 6, no. 8, pp. 893–903, Nov. 2022.

[33] G. Gallina et al., "Characterization of the Hamamatsu VUV4 MPPCs for nEXO," *Nucl. Instrum. Methods Phys. Res. A, Accelerators Spectrometers Detect. Assoc. Equip.*, vol. 940, pp. 371–379, Oct. 2019.

[34] P. Kadkhoda, D. Ristau, and F. von Alvensleben, "Total scatter measurements in the DUV/VUV," in *Proc. Laser-Induced Damage Opt. Mater.*, 1999, p. 544.

[35] S. Gundacker, A. Knapitsch, E. Auffray, P. Jarron, T. Meyer, and P. Lecoq, "Time resolution deterioration with increasing crystal length in a TOF-PET system," *Nucl. Instrum. Methods Phys. Res. A, Accelerators Spectrometers Detect. Assoc. Equip.*, vol. 737, pp. 92–100, Feb. 2014. [Online]. Available: http://dx.doi.org/10.1016/j.nima.2013.11.025

[36] C. Casella, M. Heller, C. Joram, and T. Schneider, "A high resolution TOF-PET concept with axial geometry and digital SiPM readout," *Nucl. Instrum. Methods Phys. Res. A, Accelerators Spectrometers Detect. Assoc. Equip.*, vol. 736, pp. 161–168, Feb. 2014. [Online]. Available: http://dx.doi.org/10.1016/j.nima.2013.10.049